Conference on Modelling Fluid Flow (CMFF'25)
The 19th International Conference on Fluid Flow Technologies
Budapest, Hungary, August 26-August 29, 2025

EVALUATION OF CAROTID PLAQUE MORPHOMETRY AND HEMODYNAMICS

Benjamin CSIPPA[1], Márton NÉMETH[1], György PAÁL[1], Zsuzsanna MIHÁLY[2]

[1] Department of Hydrodynamic Systems, Faculty of Mechanical Engineering, Budapest University of Technology and Economics. Műegyetem rkp. 3., H-1111, Budapest, Hungary. E-mail: bcsippa@hds.bme.hu (Corresponding Author), mnemeth@hds.bme.hu, paal@hds.bme.hu
[2] Department of Vascular Surgery, Heart and Vascular centre, Faculty of Medicine, Semmelweis University. E-mail: mihaly.zsuzsanna@med.semmelweis-univ.hu

ABSTRACT

Carotid artery disease is a narrowing in the vessel that forms due to the accumulation of plaque material on the wall of the vessel. These obstructions present a risk of stroke and decrease blood flow into the brain circulation. One of the usual treatments is carotid endarterectomy when a vascular surgeon removes the plaque during open wound surgery.

In this study, we are interested in the relationship between plaque morphometry and hemodynamics in the arterial section. For this purpose, we must develop a capable evaluation technique encompassing the hemodynamic and morphometric quantities in a common reference frame along the arterial centerline. Previously, we developed a solution to evaluate hemodynamic quantities in the geometrical framework of the centerline. Now, we extend this framework to include the geometrical characterization of the plaque morphometry.

Data on plaque morphometry were acquired with VascuCap (now ElucidVivo), a commercial tool that automatically detects plaque characteristics from CT images of the carotid artery. The hemodynamics is calculated with the finite-volume solver of Ansys CFX. With this technique, we can connect the properties of the plaque material to the hemodynamic indices and understand how the characteristics of the plaque material are connected to the dynamic load of the fluid.

Keywords: carotid artery, CFD, hemodynamics, plaque morphometry

NOMENCLATURE

CEA	$[-]$	Carotid endarterectomy
div_W	$[-]$	Wall Shear Stress divergence
LSA	$[-]$	Low time-averaged WSS area
OSI	$[-]$	Oscillatory Shear Index
$\underline{\tau}$	$[Pa]$	wall shear stress vector
$\underline{e}$	$[-]$	wall cell unit vectors
$\underline{FR_t}$	$[-]$	Frenet tangent unit vector
WSS	$[Pa]$	Wall Shear Stress
C	$[m^3/Pa]$	compliance
R_1	$[Pas/m^3]$	Proximal resistance
R_2	$[Pas/m^3]$	distal resistance

Subscripts and Superscripts
b, n, t normal, binormal, tangential

1. INTRODUCTION

Wall Shear Stress (WSS) characterisation of the carotid artery bifurcation has been the centre of scrutiny for a number of years as it has been identified to be linked with atherosclerosis [1, 2, 3] . Carotid stenosis can present a severe risk for stroke since, in the event of plaque rupture, the lipid-rich necrotic core can enter the bloodstream, causing a blockage in the distal vasculature. Treatment can be either vascular stenting or carotid endarterectomy (CEA). In the case of CAE, the surgeon removes the plaque entirely with an open wound surgery, reconstructing the bifurcation. In the literature, research has investigated a number of WSS metrics to identify possible susceptibility factors for carotid stenosis or even the risk of long-term restenosis. Low time-averaged WSS area (LSA) and oscillatory WSS index (OSI) are significant independent risk factors. Furthermore, recently, the divergence of the time-averaged WSS vector field (div_W) gained significant interest as div_W can show the topological skeleton of the WSS field [4] by identifying WSS fixed points and corresponding stable/unstable manifolds around the contraction and expansion regions.

The present study explores and expands these WSS metrics by further analysing the WSS field according to the vessel centerline direction to understand the effect of WSS directionality. WSS directionality was previously proposed by [5], yet not in the context of analysing the hemodynamics of the carotid artery stenosis. This pilot study ties together several evaluation metrics to understand the hemo-

Copyright© Department of Fluid Mechanics, Budapest University of Technology and Economics and the Authors

dynamic behaviour affecting the vascular biology.

Additionally, plaque morphometry was calculated using VascuCap, the CT-based technology from Elucid Bio. The aim is to connect the information on plaque composition with hemodynamic modeling to understand the formation of atherosclerotic lesions. In this pilot study, the necessary workflow was built to evaluate the plaque morphometry within the same computational coordinate system of the hemodynamic simulation. In the future, the objective is to analyse a larger patient cohort with the developed methods.

2. METHODS

2.1. Geometry & CFD

A patient who underwent CEA procedure at the Heart and Vascular centre of Semmelweis University were selected for this study. The hospital ethics committee approved the study, and patients provided informed consent. CT-angiography was performed to obtain the pre-CEA and post-CEA 3D geometry by manual segmentation in Slicer (www.slicer.org), followed by surface mesh post-processing in the Vascular Modeling Toolkit (VMTK, www.vmtk.org). The pre-CEA images were used for the VascuCap analysis. The analysis only captured the ICA side of the bifurcation in a range set by the operator, a vascular surgeon. Multiple regions of vasculature and plaque can be analysed with the technology, but for this study, only the plaque composition was used. Namely, the calcified (Ca*) and the lipid-rich necrotic core (LRNC) regions. The pre-and post-CEA geometries with the pre-CEA plaque composition can seen in Figure 1.

Transient CFD simulations were carried out using the ANSYS CFX solver based on the finite volume method. Numerical meshes were created in ANSYS, containing approximately 5 million tetrahedral numerical cells with seven prismatic layers next to the vessel wall. In the present study, mesh independence was not studies. According to the literature, a numerical mesh containing five million numerical cells is well above the usual considerations[6]. Here, we adopted the larger mesh count to adeaquatley calculate the divergence of the WSS. Blood was modeled as a homogenous Newtonian fluid with a density and viscosity of 1055 kg/m^3 and 3.4 $mPa\ s$, respectively. Since the Reynlods numbers are below 1500, it was assumed that the flow is laminar, hence tubulence models were not considered for the simulations. The vessel wall as assumed to be rigid, which is a usual assumption in the literature. Doppler ultrasound velocimetry was used to extract velocity waveforms at the CCA before CEA and used as inlet boundary conditions for the transient simulations. Three-element Windkessel outlet boundary conditions [7] were set on the internal and external carotid arteries (ICA, ECA) with the following parameters:

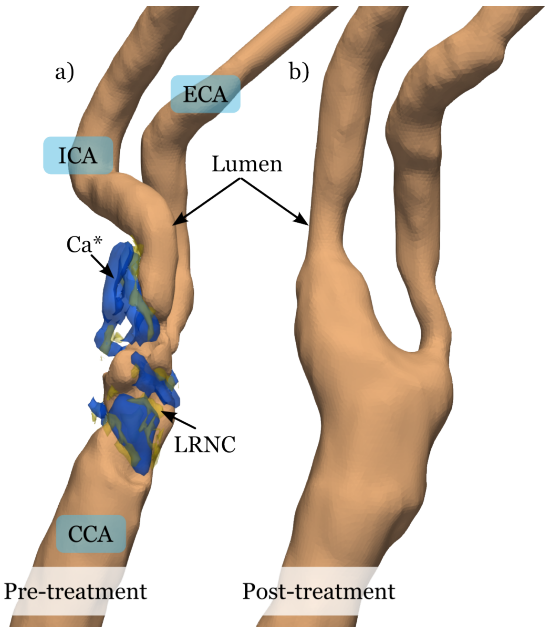

Figure 1. Patient-specific geometry before (a) and after (b) the endarterectomy procedure. Besides the lumen (fluid domain), the calcified (Ca*) region and the lipid-rich necrotic core (LRNC) are visualized with opaque blue and yellow surfaces.

Table 1. Three-element Windkessel paramaters. Proximal resistance R_1, distal resistance R_2 and compliance C for the internal and external carotid artery boundary.

	R_1 $[Pas/m^3]$	R_2 $[Pas/m^3]$	C $[m^3/Pa]$
ICA	10^8	10^9	10^{-10}
ECA	10^9	10^{10}	10^{-11}

Second-order spatial and temporal discretisation schemes were used, and 5000 time steps were simulated [8]. Three cardiac cycles were computed, and the last was used for further evaluation. The results were exported in vtk format for post-processing with our Python-based workflow.

2.2. WSS characterization

The PyVista Python package was used to develop automated evaluations. Since the WSS field will be evaluated, the surface elements were only extracted from the numerical domain. The unit vectors normal to the wall e_n were calculated for each numerical cell on the surface. Similarly, as in Arzani and Shadden [5], to construct an intrinsic orthonormal coordinate frame (e_n, e_t, e_b) to follow the centerline direction that varies along the vessel surface. The tangential unit vector e_t that mostly aligns with the centerline tangent vector Fr_t can be calculated as follows:

$$\mathbf{e_t} = \frac{\mathbf{Fr_t} - (\mathbf{Fr_t} \cdot \mathbf{e_n})\mathbf{e_n}}{\|\mathbf{Fr_t} - (\mathbf{Fr_t} \cdot \mathbf{e_n})\mathbf{e_n}\|} \tag{1}$$

Copyright© Department of Fluid Mechanics, Budapest University of Technology and Economics and the Authors

where $\mathbf{Fr_t}$ is the tangent unit of the closest centerline point transfered to the associated surface cell. Corresponding centerline points and the associated $\mathbf{Fr_t}$ unit vectors are calculated using the CKDTree algorithm and transferred as a vector field on the surface to compute the above equation for each cell. Consequantly, the $\mathbf{e_b}$ the binormal unit vector can be calculated as $\mathbf{e_b} = \mathbf{e_t} \times \mathbf{e_n}$. Using these unit vectors, the WSS vector can be decomposed into a tangential and a binormal direction as:

$$\boldsymbol{\tau} = (\boldsymbol{\tau} \cdot \mathbf{e_t})\mathbf{e_t} + (\boldsymbol{\tau} \cdot \mathbf{e_b})\mathbf{e_b} = \boldsymbol{\tau}_t + \boldsymbol{\tau}_b \tag{2}$$

Here, we want to remark that the decomposition is only valid for the CCA before the bifurcation and on the ICA side since only the centerline going from the CCA to the ICA was considered in this pilot study. The integral average along the cardiac cycle can compute the time-averaged quantities:

$$\|\overline{\boldsymbol{\tau}_t}\| = \left\| \frac{1}{T} \int_0^T \boldsymbol{\tau}_t dt \right\| \tag{3}$$

and for $\|\overline{\boldsymbol{\tau}_b}\|$:

$$\|\overline{\boldsymbol{\tau}_b}\| = \left\| \frac{1}{T} \int_0^T \boldsymbol{\tau}_b dt \right\| \tag{4}$$

Figure 2 demonstrates the the $\overline{\boldsymbol{\tau}_t}$ and $\overline{\boldsymbol{\tau}_b}$ vector fields using the Post-CEA geometry as an example.

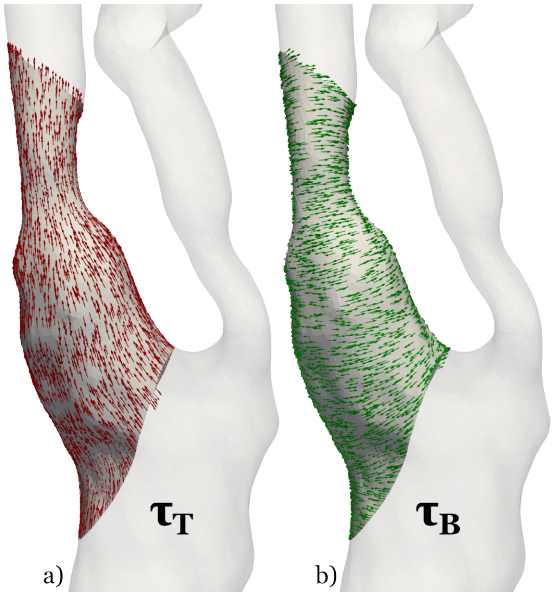

Figure 2. $\overline{\boldsymbol{\tau}_t}$ (a) and $\overline{\boldsymbol{\tau}_b}$ (b) vector fields on the luminal surface of the post-CEA geometry.

Continuing with the definition of the usual WSS parameters used in the literature: $\|\overline{\boldsymbol{\tau}}\|$ is the magnitude of the cycle-averaged WSS vector:

$$\|\overline{\boldsymbol{\tau}}\| = \left\| \frac{1}{T} \int_0^T \boldsymbol{\tau} dt \right\| \tag{5}$$

The time-averaged WSS magnitude is defined as:

$$TAWSS = \frac{1}{T} \int_0^T \|\boldsymbol{\tau}\| dt \tag{6}$$

where T is the time of the cardiac cycle. The oscillatory shear index (OSI) is as follows:

$$OSI = \frac{1}{2}\left(1 - \frac{\|\overline{\boldsymbol{\tau}}\|}{TAWASS}\right) \tag{7}$$

Finally, the divergence of the WSS vector can be calculated to visualize the WSS contraction and expansion regions:

$$div_W = \nabla \cdot \hat{\boldsymbol{\tau}} \tag{8}$$

where $\hat{\boldsymbol{\tau}}$ is the normalized instantaneous WSS vector field on the luminal surface. In the following, an example of the use of these metrics will be demonstrated on the carotid geometry of the patient. Pre-CEA and post-CEA visualizations are confined to the domain close to the carotid bifurcation region. Plaque composition will only be shown for the OSI and div_W metrics to showcase the connection with the WSS vectorial behavior.

3. RESULTS & DISCUSSION

In Figure 3, a threshold area of the TAWSS field can be seen as the Low Shear Area (LSA) corresponding to regions where TAWSS is lower than 3 *Pa*. There is a clear difference between the pre-CEA and post-CEA LSA variation.

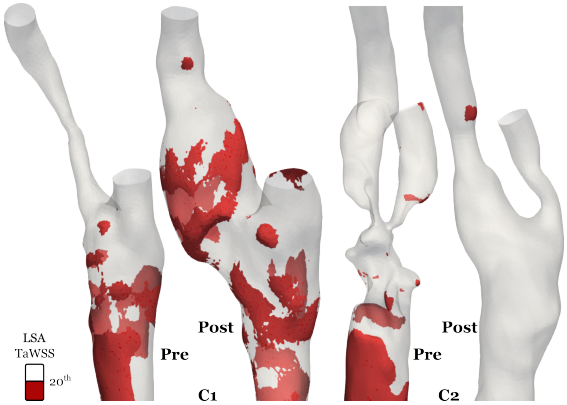

Figure 3. Low WSS area (LSA) with a threshold set at 20th percentile of TaWSS of the accumulated all values from all cases, before (a) and after (b) the CEA procedure.

In the diseased state, multiple recirculation zones are present due to the shape modification of severe stenosis. Following the CEA procedure, these spots of recirculation zones disappeared as the carotid bulb was reconstructed, and only one large vortical region was present in the bulb. A further change in LSA can be attributed to the geometrical difference between

Copyright© Department of Fluid Mechanics, Budapest University of Technology and Economics and the Authors

the parent artery before and after the CEA procedure. The shape of the ICA significantly changed after the procedure as the artery became less tortuous, hence the more uniform flow features and WSS field.

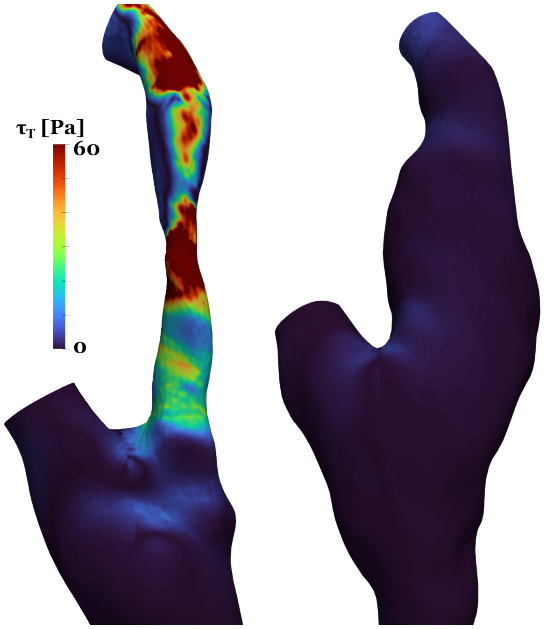

Figure 4. Time-averaged tangential WSS vector field $\|\overline{\tau_t}\|$, before (a) and after (b) the CEA procedure for case C1.

In Figure 4, 5 and 6, 7 the time-averaged decomposition of the WSS field can be seen, the $\|\overline{\tau_t}\|$ and $\|\overline{\tau_b}\|$, respectively. In the stenosis region, both the tangential and binormal components indicate a strong swirling flow, possibly due to the complex shape of the lumen in the atherosclerotic carotid bulb. Disturbed flow features emerge due to the deformed shape of the lumen at the carotid bulb. Therefore, the magnitude of both the tangential and binormal components of the WSS field is high in this region since the inflow region is highly disturbed. It can be seen that before the stenosis, the binormal component dominates as small-scale counter-rotating recirculation zones precede in the different pockets, depicted by the lines of near-zero $\|\overline{\tau_b}\|$ values where the WSS vector component changes direction.

The binormal and tangential WSS on the luminal surface also show that after the CEA procedure, the tangential WSS component will dominate in the slightly stenosed vessel segment. The binormal $\|\overline{\tau_b}\|$ component decreased substantially in the stenosis as less disturbed flow enters the narrowing region. The reconstruction after the CEA procedure of the carotid bulb fundamentally changed the flow and WSS field. Due to the decreased velocity in the segment, the tangential component becomes directionally stable without large zones of backflow. The binormal component displays the expected features of the secondary flow phenomenon as a consequence of the bifurcation. The topology of the WSS vector

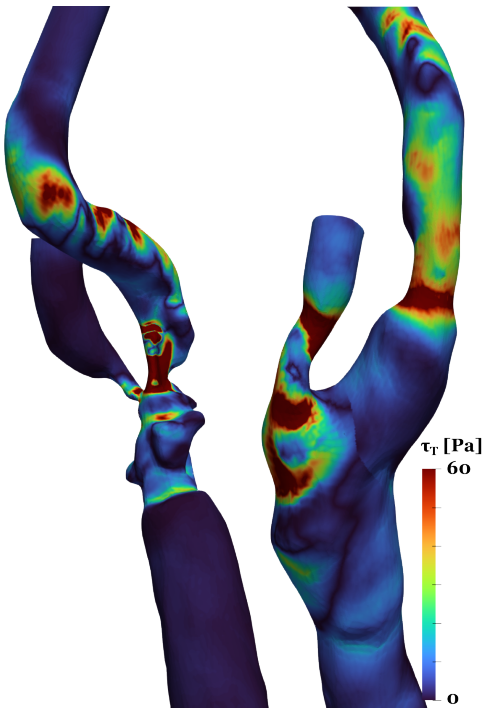

Figure 5. Time-averaged tangential WSS vector field $\|\overline{\tau_t}\|$, before (a) and after (b) the CEA procedure for case C2.

field after the CEA procedure resembles what would be expected in a healthy state. However, further investigation is needed to understand long-term outcomes in the presence of mild stenosis after the reconstruction.

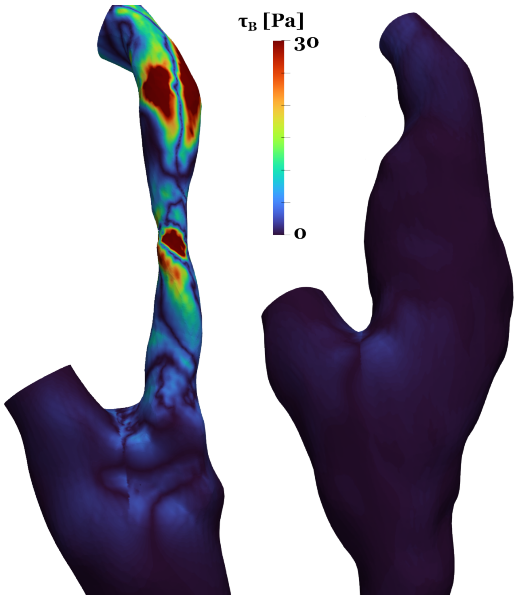

Figure 6. Time-averaged tangential WSS vector field $\|\overline{\tau_b}\|$, before (a) and after (b) the CEA procedure for case C1.

Copyright© Department of Fluid Mechanics, Budapest University of Technology and Economics and the Authors

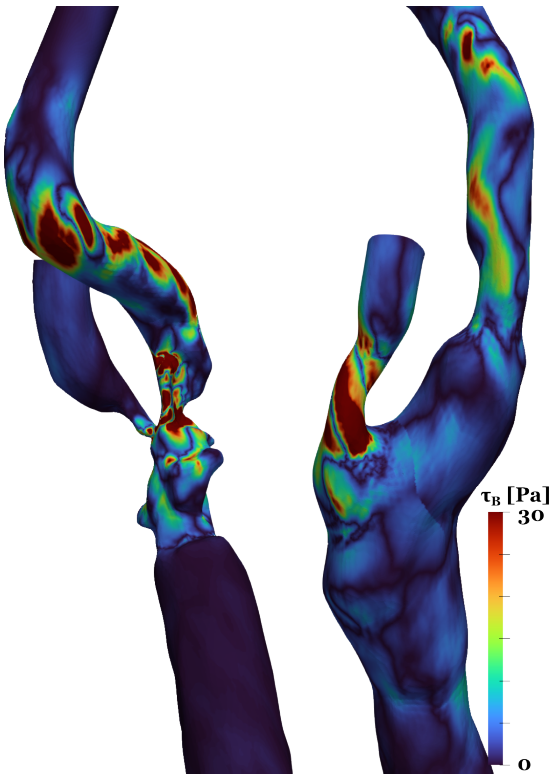

Figure 7. Time-averaged tangential WSS vector field $\|\overline{\tau_b}\|$, before (a) and after (b) the CEA procedure for case C2.

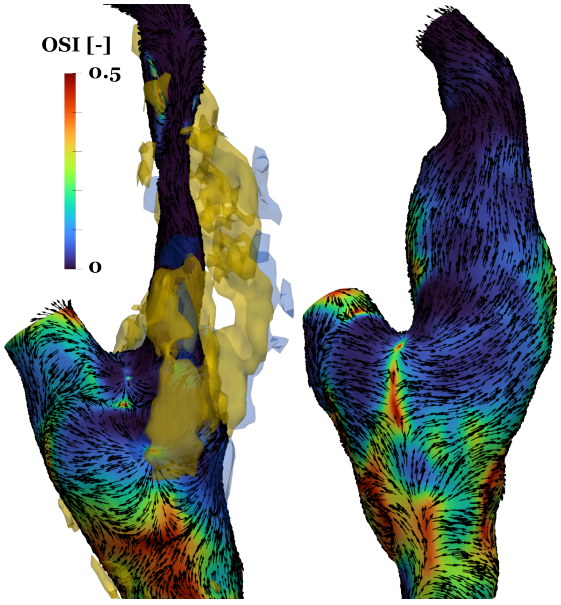

Figure 8. Oscillatory Shear Index (OSI) on the luminal surface for case C1. The time-averaged WSS field is visualized by normalized arrows (black). Besides the lumen (fluid domain), the calcified (Ca*) region and the lipid-rich necrotic core (LRNC) are visualized with opaque blue and yellow surfaces.

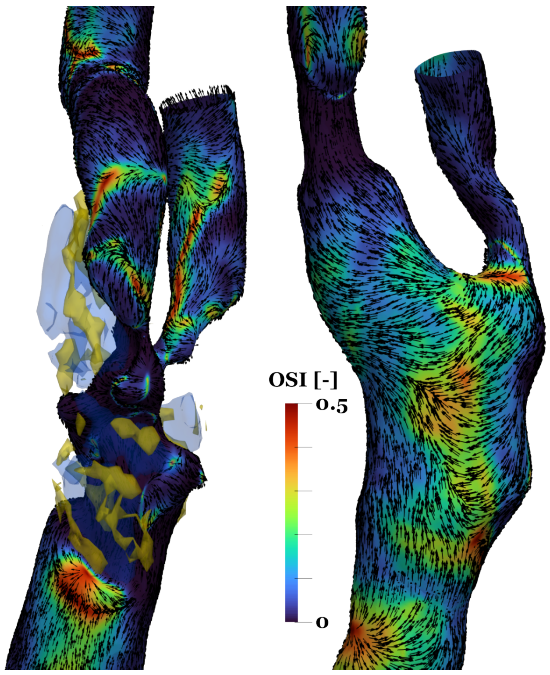

Figure 9. Oscillatory Shear Index (OSI) on the luminal surface for case C1. The time-averaged WSS field is visualized by normalized arrows (black). Vector visualization according to the previous image.

In Figure 8 and 9, the temporal behavior of the WSS field is expressed with the oscillatory shear index. By definition, the index measures the temporal variability of the pointwise directionality change of the WSS vectors. Close to zero values correspond to stable WSS vector directionality, while close to 0.5, the vector has no preferred directions throughout the cardiac cycle. The largest difference comparing the diseased and surgically reconstructed cases is the apparent small values of OSI in the atherosclerotic regions. Case 1: Large regions of oscillatory behaviour can be observed, known to be susceptible to later restenosis formation [9]. Another observation based on OSI maps is that the plaque material accumulated mostly in regions of low OSI. However, a cause-and-effect relationship cannot be drawn from the observation, as the formation of atherosclerotic plaques is not yet understood.

In Figure 10 and 11, the divergence of the WSS vector field can be observed. The WSS contraction/expansion regions are denoted with colder/warmer colors. According to our observations, stronger contraction regions were identified in the atherosclerotic region, both in the carotid bulb and near the stenosis. The post-CEA cases display a stronger expansion region at the apex of the bifurcation and only weaker contraction regions in the carotid bulb. The effect of expansion/contraction on vascular biology needs further quantitative analysis, as according to the literature [4, 2], this WSS-related

Copyright© Department of Fluid Mechanics, Budapest University of Technology and Economics and the Authors

action can be connected to the formation of atherosclerosis.

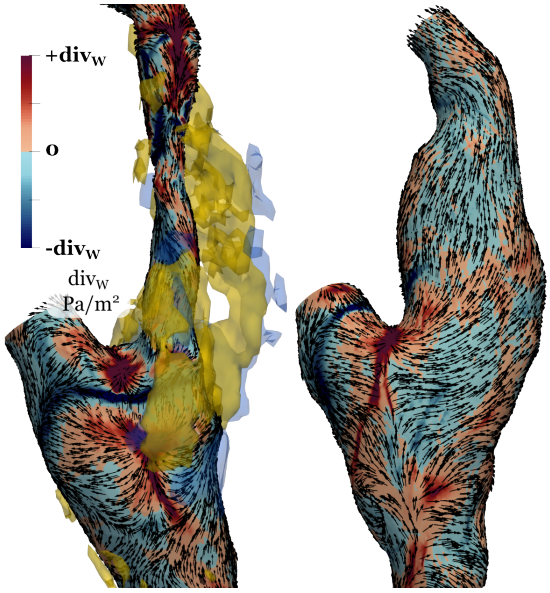

Figure 10. Wall Shear Stress divergence (div_W) on the luminal surface for case C1. The time-averaged WSS field is visualized by normalized arrows (black). Besides the lumen (fluid domain), the calcified (Ca*) region and the lipid-rich necrotic core (LRNC) are visualized with opaque blue and yellow surfaces.

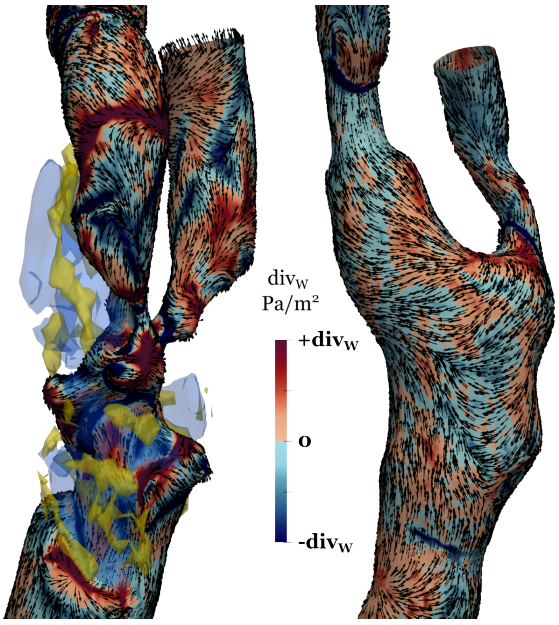

Figure 11. Wall Shear Stress divergence (div_W) on the luminal surface for case C2. Vector visualization according to the previous image.

4. SUMMARY

This pilot study investigates the relationship between plaque morphometry and hemodynamics in the carotid artery, focusing on patients undergoing carotid endarterectomy (CEA). An evaluation method was developed to analyze the interaction between plaque composition and blood flow dynamics, integrating morphometric data from VascuCap (now ElucidVivo) with hemodynamic simulations. Wall shear stress (WSS) characterization was achieved by decomposing the vector field along the vessel centerline to understand the emergence of globally interpreted standard hemodynamic parameters, including time-averaged WSS (TAWSS), oscillatory shear index (OSI), and WSS divergence (div_W). This new insight can shed light on the interplay between directional WSS metrics, oscillatory behaviour [10], and vascular biology. The results demonstrated that CEA significantly alters the WSS field, reducing the spurious appearance of low-shear areas and stabilizing flow patterns. The reconstructed artery exhibited a more uniform WSS distribution, particularly in regions previously affected by stenosis.

This pilot study established the methodology for integrating morphometric and hemodynamic data within a unified computational framework. Future work will expand the analysis to a larger patient cohort to understand the cause-and-effect relationship between hemodynamic metrics and plaque formation.

ACKNOWLEDGEMENTS

This research was funded by NKFI-PD23 146299 grant between 2024 and 2027. NKFI: Nemzeti Kutatási Fejlesztési és Innovációs Hivatal/ National Research, Innovation and Development Office

REFERENCES

[1] Gallo, D., Steinman, D. A., and Morbiducci, U., 2016, “Insights into the co-localization of magnitude-based versus direction-based indicators of disturbed shear at the carotid bifurcation”, *Journal of biomechanics*, Vol. 49 (12), pp. 2413–2419.

[2] Morbiducci, U., Mazzi, V., Domanin, M., De Nisco, G., Vergara, C., Steinman, D. A., and Gallo, D., 2020, “Wall shear stress topological skeleton independently predicts long-term restenosis after carotid bifurcation endarterectomy”, *Annals of biomedical engineering*, Vol. 48, pp. 2936–2949.

[3] Lee, S.-W., Antiga, L., Spence, J. D., and Steinman, D. A., 2008, “Geometry of the carotid bifurcation predicts its exposure to disturbed flow”, *Stroke*, Vol. 39 (8), pp. 2341–2347.

[4] Mazzi, V., Gallo, D., Calò, K., Najafi, M., Khan, M. O., De Nisco, G., Steinman,

Copyright© Department of Fluid Mechanics, Budapest University of Technology and Economics and the Authors

D. A., and Morbiducci, U., 2020, "A Eulerian method to analyze wall shear stress fixed points and manifolds in cardiovascular flows", *Biomechanics and Modeling in Mechanobiology*, Vol. 19 (5), pp. 1403–1423.

[5] Arzani, A., and Shadden, S. C., 2016, "Characterizations and correlations of wall shear stress in aneurysmal flow", *Journal of biomechanical engineering*, Vol. 138 (1), p. 014503.

[6] El Sayed, R., Sharifi, A., Park, C. C., Haussen, D. C., Allen, J. W., and Oshinski, J. N., 2023, "Optimization of 4D flow MRI spatial and temporal resolution for examining complex hemodynamics in the carotid artery bifurcation", *Cardiovascular engineering and technology*, Vol. 14 (3), pp. 476–488.

[7] Vignon-Clementel, I. E., Figueroa, C., Jansen, K., and Taylor, C., 2010, "Outflow boundary conditions for 3D simulations of non-periodic blood flow and pressure fields in deformable arteries", *Computer methods in biomechanics and biomedical engineering*, Vol. 13 (5), pp. 625–640.

[8] Mancini, V., Bergersen, A. W., Vierendeels, J., Segers, P., and Valen-Sendstad, K., 2019, "High-Frequency Fluctuations in Post-stenotic Patient Specific Carotid Stenosis Fluid Dynamics: A Computational Fluid Dynamics Strategy Study", *Cardiovasc Eng Technol*, Vol. 10 (2), pp. 277–298.

[9] Domanin, M., Gallo, D., Vergara, C., Biondetti, P., Forzenigo, L. V., and Morbiducci, U., 2019, "Prediction of long term restenosis risk after surgery in the carotid bifurcation by hemodynamic and geometric analysis", *Annals of biomedical engineering*, Vol. 47, pp. 1129–1140.

[10] Morbiducci, U., Kok, A. M., Kwak, B. R., Stone, P. H., Steinman, D. A., and Wentzel, J. J., 2016, "Atherosclerosis at arterial bifurcations: evidence for the role of haemodynamics and geometry", *Thrombosis and haemostasis*, Vol. 115 (03), pp. 484–492.

Copyright© Department of Fluid Mechanics, Budapest University of Technology and Economics and the Authors